Optical suppression of tilt-to-length coupling in the LISA long-arm interferometer

M Chwalla,[1] K Danzmann,[2] M Dovale Álvarez,[2, *] J J Esteban Delgado,[2] G Fernández Barranco,[2]
E Fitzsimons,[1, 3] O Gerberding,[2, 4] G Heinzel,[2] C J Killow,[5] M Lieser,[2] M Perreur-Lloyd,[5]
D I Robertson,[5] S Schuster,[2] T S Schwarze,[2] M Tröbs,[2] G Wanner,[2] H Ward,[5] and M Zwetz[2]

[1]*Airbus DS GmbH, Claude-Dornier-Straße, 88090 Immenstaad, Germany*
[2]*Max Planck Institute for Gravitational Physics (Albert Einstein Institute) and Institute for
Gravitational Physics of the Leibniz Universität Hannover, Callinstraße 38, 30167 Hannover, Germany*
[3]*UK Astronomy Technology Centre, Royal Observatory Edinburgh, Blackford Hill, Edinburgh EH9 3HJ, UK*
[4]*Institute for Experimental Physics, University of Hamburg, Luruper Chaussee 149, 22761, Hamburg, Germany*
[5]*SUPA, Institute for Gravitational Research, University of Glasgow, Glasgow G12 8QQ, Scotland, UK*

The arm length and the isolation in space enable LISA to probe for signals unattainable on ground, opening a window to the sub-Hz gravitational-wave universe. The coupling of unavoidable angular spacecraft jitter into the longitudinal displacement measurement, an effect known as tilt-to-length (TTL) coupling, is critical for realizing the required sensitivity of picometer/$\sqrt{\text{Hz}}$. An ultra-stable interferometer testbed has been developed in order to investigate this issue and validate mitigation strategies in a setup representative of the LISA long-arm interferometer. We demonstrate a reduction of TTL coupling between a flat-top beam and a Gaussian beam via introducing two- and four-lens imaging systems. TTL coupling factors below $\pm 25\,\mu\text{m/rad}$ for beam tilts within $\pm 300\,\mu\text{rad}$ are obtained by careful optimization of the system. Moreover we show that the additional TTL coupling due to lateral alignment errors of elements of the imaging system can be compensated by introducing lateral shifts of the detector, and vice versa. These findings help validate the suitability of this noise-reduction technique for the LISA long-arm interferometer.

I. INTRODUCTION

Directly sensing gravitational effects by tracking the motion between freely moving masses is at the center of experimental gravitational physics, with various exciting results achieved in recent years. On 14 September 2015 the Laser Interferometer Gravitational-Wave Observatory (LIGO) [1], consisting of two second generation detectors listening in the Hz to kHz band, made the first direct observation of gravitational waves from a binary black hole merger (GW150914) [2]. The discovery consolidated laser interferometry as a suitable technology for gravitational-wave detection, and strengthened the revolutionary scientific value and discovery potential of a deep-space gravitational-wave observatory capable of listening to sub-Hz gravitational-wave signals, such as the Laser Interferometer Space Antenna (LISA) [3, 4].

On 3 December 2015 the European Space Agency (ESA) launched LISA Pathfinder (LPF), a single satellite technology demonstrator for LISA, providing successful flight demonstration of critical LISA-like instruments [5–7]. On 22 May 2018, the National Aeronautics and Space Administration (NASA) and the German Research Centre for Geosciences (GFZ) launched GRACE Follow-On (GRACE-FO), a twin satellite gravity exploration mission carrying a laser ranging instrument, successfully proving LISA-like technologies for inter-spacecraft optical links, albeit on a much smaller baseline of only 200 km [8].

LISA has been approved by ESA as the ESA-L3 Gravitational Wave Mission [9], and while it will feature flight-proven instruments and interferometry techniques, it also presents many new technical challenges. The LISA long-arm interferometer features the longest baseline of any human-made gravity and spacetime experiment in history with approximately 2.5 million kilometers. LISA will be able to probe a large and as-yet unexplored part of the *gravitational universe*, measuring gravitational waves in a frequency band (0.1 mHz to 1 Hz) where current ground-based laser interferometers, such as LIGO or Virgo, have poor sensitivity [10]. The unprecedented laser interferometric baseline in combination with the desired precision, however, presents unique challenges that can be considered fundamental for such measurement schemes.

The LISA satellites exchange laser signals that probe the displacement between the satellites' free-floating test masses in order to detect spacetime strain between the spacecraft. A locally generated Gaussian beam is emitted via a telescope, propagates through the $\sim 2.5 \cdot 10^9$ m-long interferometer arm, and is captured by a similar telescope in the remote spacecraft. The received light, which is the result of clipping the center region of a kilometer-scale light beam with a small aperture, is interfered with the local beam, and their heterodyne beat is used to obtain a measurement of the length fluctuations of the arms with picometer/$\sqrt{\text{Hz}}$ precision, encoding the gravitational-wave signal.

This measurement is challenged by many noise sources at the local instrument level, at the optical link level, and of residual origin. Tilt-to-length coupling is one of the most significant contributions to the total noise budget in LISA (and also in LPF [11] and GRACE-FO [12, 13]). Relative angular motion between the test mass and spacecraft, and between remote spacecraft, results in angular jitter of the interfering beams and a consequent error in the longitudinal displacement measurement.

In LISA, TTL coupling noise is expected to be very significant, with a large contribution stemming from the long arm interferometer, partly due to the magnification provided by
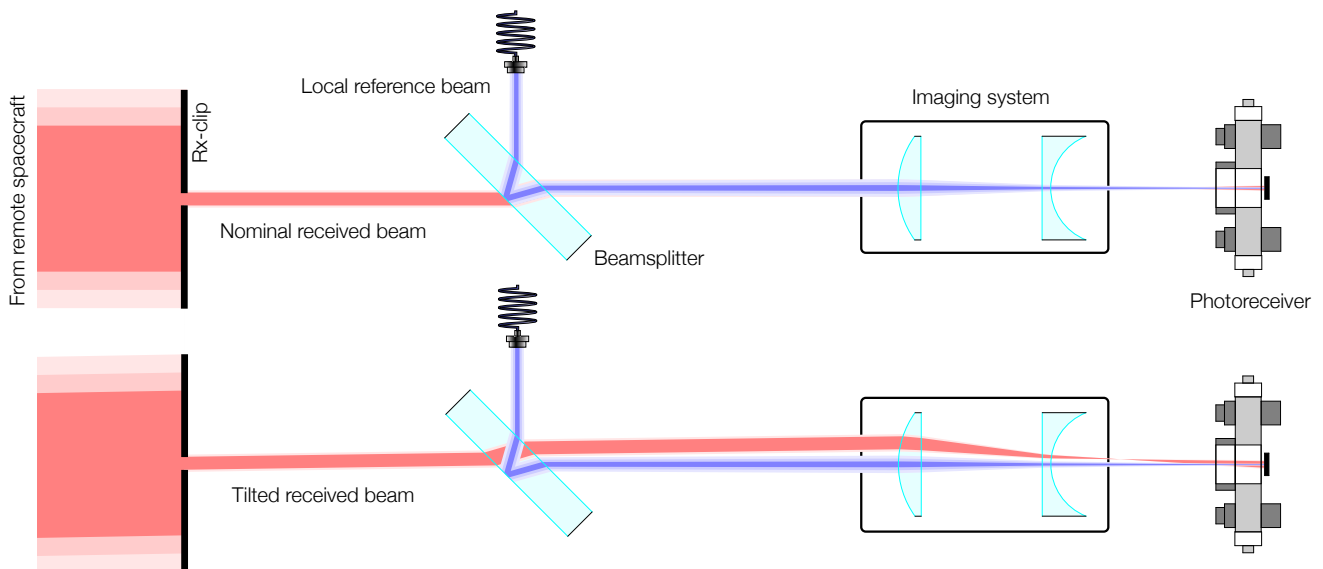
* miguel.dovale@aei.mpg.de

FIG. 1. Tilt-to-length coupling in the LISA long-arm interferometer. *Top:* The received beam, that propagated through the ∼ $2.5 \cdot 10^9$ m-long arm, is captured by a telescope and imaged onto the Rx-clip, a small aperture located in the optical bench. The received light, which has a flat-top profile as a result of clipping the large beam at a small circular aperture, interferes with a locally generated Gaussian beam, and their heterodyne beat note — encoding the gravitational-wave signal — is registered by a quadrant photodiode. *Bottom:* Angular jitter of the spacecraft causes a tilt of the Rx beam with respect to the Rx-clip, and a consequent error in the longitudinal pathlength signal measurement, a source of noise known as tilt-to-length coupling (the tilt has been exaggerated in the figure for illustration). Imaging systems can be used to image the Rx-clip onto the detector plane, hence reducing TTL coupling in the interferometer and increasing LISA's robustness to alignment noise.

the telescope, which increases the tilt sensed by the photoreceivers. Therefore, a system for suppressing this cross-talk is essential. One such approach is to use imaging systems to image the tilting beams onto the photoreceivers. In the long-arm interferometer, angular motion of the spacecraft translates into tilt of the measurement beam with respect to a fixed aperture on the optical bench, the Rx-clip. Thus, an optical system configured to image the Rx-clip onto the detectors can significantly lower the impact of this noise source in the interferometer (Figure 1).

In this paper we present an investigation of TTL coupling noise reduction in the LISA long-arm interferometer via two- and four-lens imaging systems. A testbed has been developed which incorporates a pair of ultra-stable Zerodur interferometer platforms. The testbed has been used previously to show that the imaging systems reduced TTL coupling in the test mass interferometer to within $\pm 25 \, \mu$m/rad (i.e., ± 1 pm/40 nrad) for beam tilt angles within $\pm 300 \, \mu$rad, a performance requirement derived from a top-level breakdown carried out in a previous mission study [14]. The long-arm interferometer, however, presents a unique challenge due to the nature of the received light, which has a flat amplitude and phase profile [15–18]. The interference between the flat-top beam, after it undergoes diffraction at the aperture and is imaged onto the detector, and the reference Gaussian beam, is fundamentally different from the interference between two Gaussian beams. We demonstrate that TTL coupling suppression with imaging systems still meets the required performance in the long-arm interferometer, albeit further opti-

mization is necessary. Furthermore, we demonstrate that the residual TTL coupling of the imaging system can be counteracted by intentionally misaligning the system.

Section II presents the measurement concept and the layout of the testbed and relevant subsystems. An introduction to tilt-to-length coupling noise, and to the suppression mechanism investigated in this paper, is given in Section III. Section IV provides the experimental results and the achieved performance of the imaging systems. Additionally, the robustness of the setup against alignment errors of the system was investigated and a tolerance analysis is provided.

II. LISA OPTICAL BENCH TESTBED

The LISA Optical Bench (LOB) [19], of which there are two per spacecraft, will likely consist on an ultra low expansion glass baseplate to which other optical elements are bonded via hydroxide-catalysis bonding [20]. The LOB hosts critical components of the different interferometers that make up the LISA detector. The long-arm (LA) interferometer tracks the relative length fluctuations between satellites by measuring the relative phase between the long-traveled received beam (Rx) and a locally generated beam (Tx), as well as the relative alignment via the differential wavefront sensing (DWS) signals [21, 22]. The test mass (TM) interferometer measures the longitudinal displacement between the test mass and the LOB using the Tx beam and another locally generated beam (LO), as well as the tilt of the test mass via DWS.
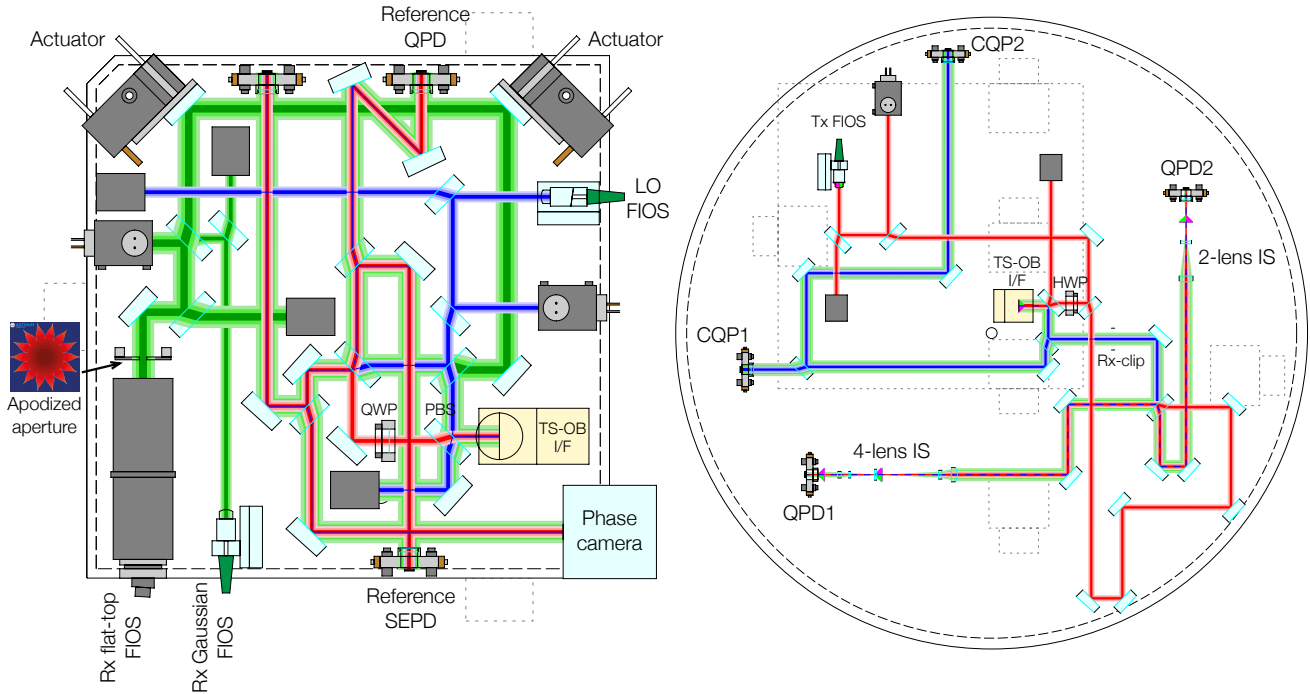
FIG. 2. Layout of the testbed. *Left:* The telescope simulator (TS) provides the optical bench (OB) with laser beams (Rx and LO) to simulate the LISA long-arm (LA) and test mass (TM) interferometers. To simulate the LA interferometer, a flat-top Rx beam is generated using a fiber collimator and a custom-made apodized aperture. The TS uses a three-point support system with Zerodur feet to seat on the surface of the OB, and an optical link is established via a vertical interface (TS-OB I/F). Actuated mirrors on the TS tilt the Rx beam with respect to the Rx-clip as to simulate spacecraft jitter in the LA interferometer (or test mass jitter in the TM interferometer). *Right:* In the OB, the Rx and LO beams from the TS are made to interfere along with the locally injected Tx beam, and the resulting heterodyne beat notes are read out using a balanced detection scheme with quadrant photodiodes (QPD1 and QPD2). The three beams are prepared from a frequency-doubled Nd:YAG laser (stabilized to an iodine frequency standard) that is split and passed through three acousto-optic modulators (not shown) before being injected into the TS and OB using fiber injector optical subassemblies (FIOS's). Tilts of the Rx beam translate to apparent longitudinal motion of the spacecraft or test masses, an interferometric effect referred to as tilt-to-length coupling. The effect is greatly reduced by placing specially designed imaging systems (IS's) before the QPDs. The IS reduces the optical pathlength error between the misaligned interferometric beams.

Finally, the LOB is fitted with an additional interferometer providing the phase reference between the two LOBs on one spacecraft. The measurement of the relative displacement between two distant test masses, which carries the gravitational-wave signal, is obtained by combining three contributions: the length fluctuations between the distant LOBs, and the length fluctuations between each LOB and their respective test mass.

Any effect causing alignment errors between the beams in the LA or TM interferometers (e.g., angular jitter of the spacecraft or test masses) will decrease the sensitivity in the gravitational-wave signal channel via cross-coupling of beam tilt to apparent longitudinal motion. For example, in the LA interferometer the wavefront captured by the telescope is nearly flat, but it tilts with respect to the entrance pupil of the telescope due to spacecraft angular motion. The telescope compresses the beam, imaging it onto an aperture called the Rx-clip placed on the optical bench. Therefore, angular jitter of the spacecraft manifests as tilting of the Rx beam with respect to the Rx-clip. A testbed for simulating these effects in the LOB has been developed by the Authors (see e.g., [23]), consisting of a cylindrical Zerodur optical bench (OB) and

a rectangular Zerodur telescope simulator (TS), as shown in Figure 2.

The OB, a 55 kg 580 mm-diameter 80 mm-thick Zerodur cylinder, is a simplified version of the LOB, containing only the relevant components for our investigation. The main measurement interferometer in the OB consists on a single combination beamsplitter with a balanced detection scheme, using a pair of quadrant photodiodes (QPDs) for reading out the heterodyne beat notes of either the LA or TM interferometers, depending on the input from the TS. This interferometer has a nominal optical pathlength mismatch of zero between the arms in order to minimize coupling of laser frequency noise into displacement noise. An auxiliary interferometer using a pair of calibrated quadrant photodiode pairs is also fitted for aiding alignment and calibration of the TS.

The TS provides the OB with input beams that simulate the TM and the LA interferometers, and induces angular deviations of the beams (Rx) via actuation of a pair of motorized steering mirrors. These mirrors are mounted on a custom-designed mount that suppresses any thermally induced displacements of the steering mirrors. The TS assem-
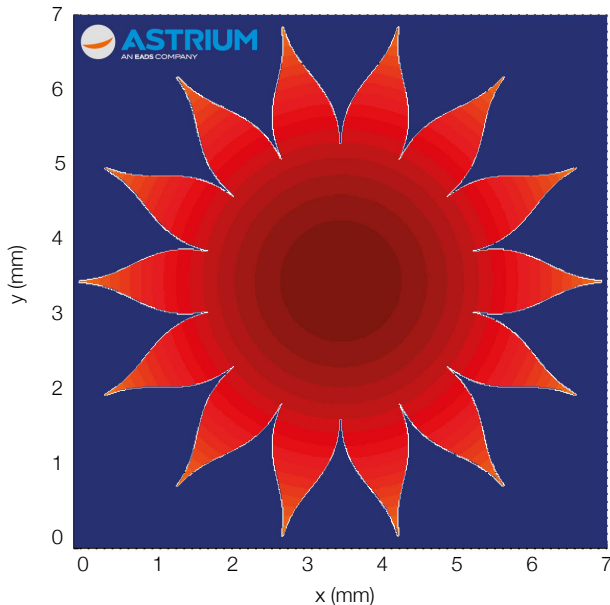
FIG. 3. Apodized aperture for flat-top beam generation. To generate a beam representative of the received beam in the LISA long-arm interferometer, a collimated 9 mm Gaussian beam is diffracted through an aperture with the shape shown. The hypergaussian "petal" shape is obtained via a Monte Carlo simulation to maximize the flatness of the diffracted beam pattern. The result is a 3 mm flat-top beam at the position of the Rx-clip.

collimator by Schäfter & Kirchhoff (60FC-T-4-M100S-37) provides a 9 mm-radius Gaussian beam that is clipped by an apodized aperture mounted at the immediate output of the collimator. The fiber collimator tube is mounted on the TS via two rings glued with flexure feet to the baseplate. The mounting structure is thermally compensated by a dual aluminum-titanium assembly, and the center of the tube is kept at a constant height to reduce beam jitter. The structure has flexures in the longitudinal and the vertical direction to avoid stress.

The shape of the aperture (Figure 3) was obtained using a Monte Carlo simulation based on maximizing the flatness of the diffracted beam pattern, which was calculated via a Fast Fourier Transform method. The best performing aperture shape was found to be the *hypergaussian*. This shape yields a transmission function that is uniform in the center and decreases beyond a certain radius with a hypergaussian dependence. The decrease is realized by the "petal" pattern, akin to a sawtooth. The theoretical transmission function never reaches zero, but the gap between adjacent petals becomes vanishingly small. The machined part, obtained from a thin $\sim 100\,\mu$m metal foil using laser etching, is limited by a minimum gap size of $20\,\mu$m.

The lateral alignment accuracy of the aperture and the effect on the resulting wavefront was investigated. The performance of the system was obtained via numerical simulation assuming a lateral alignment accuracy of $\pm 250\,\mu$m and a nominal peak-to-valley (PV) wavefront error of the collimated Gaussian beam of $\lambda/6$ over 10 mm. The resulting configuration yields an optical field with a flat wavefront (≈ 3 mm diameter) at the position of the Rx-clip. The phase flatness is $\lambda/100$ PV nominally, or up to $\lambda/25$ PV including tolerance.

A frequency doubled Nd:YAG laser based on a diode-pumped non-planar ring oscillator is locked to an iodine standard providing a 1064 nm output with an estimated frequency noise of $300\,\mathrm{Hz}/\sqrt{\mathrm{Hz}}$. The source is split in a table-top laser preparation bench and passed through three acousto-optic modulators (AOMs) to generate the three frequency components needed for the Rx, Tx and LO beams. Since the TTL coupling measurement is independent of frequency, we use heterodyne signals of few kHz, as opposed to MHz, for increased simplicity of the readout electronics. The Tx-Rx, Tx-LO, and Rx-LO beat notes are 9.765625, 14.6484375, and 24.4140625 kHz respectively, chosen to avoid harmonic relations. These signals are captured by a pair of GAP1000Q InGaAs quadrant photodiodes with 1 mm active area radius and $20\,\mu$m slit width.

For precise readout of DC components, AC amplitudes, and phase of the heterodyne signals, a custom-designed Phase Measurement System (PMS) with 16 channels has been developed, with a phase noise performance of μrad$/\sqrt{\mathrm{Hz}}$ in the 0.1 mHz to 1 Hz observation band. The DC component is proportional to the DC optical power on each QPD segment, and it is used to determine the beam positions using differential power sensing (DPS) [24]. Amplitude and phase readout are based on an in-phase/quadrature (I/Q) demodulator applied individually to each photoreceiver output channel and implemented onto a single field-programmable gate array (FPGA) for real-time operation at 80 MSPS [25].

bly, consisting of a $280\,\mathrm{mm} \times 280\,\mathrm{mm}$ rectangular Zerodur block mounted on a three-point support structure with Zerodur feet, rests on the surface of the OB, and an optical link is established between the two subsystems via a vertical interface. The TS also supplies the LO beam, which does not interact with the actuated mirrors and is used for aligning the TS to the OB.

The design of the TS (Figure 2 left) guarantees that, when it is correctly linked to the OB, any actuation of the steering mirrors causes a tilt of the Rx beam around the Rx-clip in the OB (Figure 2 right). An optical phase-locked loop (OPLL) between the LO and Rx beams, and another between the LO and Tx beams, ensures that the relative phase between the Rx and Tx beams at the Rx-clip is zero. To this end the TS is fitted with a reference photodiode in a position that is an optical copy of the Rx-clip with respect to the Rx beam (i.e., the Rx beam experiences the same phase change, geometry and motion at both locations). This is essential for ensuring that the TTL coupling measurement is free from any contributions from the TS, and only the TTL coupling that is intrinsic to the optical bench is observed. The TS has the ability to produce an Rx flat-top beam to simulate the LA interferometer, as well as a fundamental Gaussian beam to simulate the TM interferometer.

To simulate the LA interferometer, the TS must produce a flat-top beam representative of the far-field beam received from the remote spacecraft. A commercially available fiber

The raw I/Q measurements, after filtering and downsampling, are delivered to an external computer for back-end processing, computing amplitude readout as the quadrature sum of both components and phase readout as the arctangent of quadrature over in-phase. The phase of the coherent sum of all four QPD segments is used to measure longitudinal displacements with picometer precision, whereas the phases differences between pairs of QPD segments (i.e., the DWS signals) are used to compute horizontal and vertical angular signals between interfering beams with nanoradian precision. By combining the DWS and DPS signals, the control software computes a calibration matrix translating horizontal and vertical phase shifts into yaw and pitch angular tilts, respectively.

The internal clock of the PMS serves as the frequency reference to the RF signal generators that drive the AOMs, which reduces the differential clock noise between the heterodyne signals. Furthermore, the PMS is used to implement the Rx-LO, and the Tx-LO optical phase-locked loops using the single element photodiode (SEPD) in the TS. The OPLLs are based on a pair of piezo-driven mirrors placed in the optical paths of the Rx and Tx beams in the laser preparation bench before being fiber-coupled [26] into the testbed. The Rx beam can also be amplitude-modulated at 200 Hz when required to aid with the alignment of this beam in the TS and OB independently of the other beams.

The pathlength noise due to the combined readout noise sources (shot noise, electronic noise, and digitization noise) is significantly below $1 \, \mathrm{pm}/\sqrt{\mathrm{Hz}}$, given the laser power levels used in the testbed [27]. Since the investigation of TTL coupling does not require picometer stability, the testbed was operated in air and a temperature stability of $10^{-4} \, \mathrm{K}/\sqrt{\mathrm{Hz}}$ was reached using only passive thermal insulation. This translates into a pathlength noise floor of approximately $1 \, \mathrm{nm}/\sqrt{\mathrm{Hz}}$, which gives rise to an effective error in the measurement of the TTL coupling that is estimated to be on the order of $0.5 \, \mu\mathrm{m/rad}$.

III. TTL COUPLING AND IMAGING SYSTEMS

Tilt-to-length coupling in two-beam interferometers is a complex effect. *Geometric* TTL coupling originates when one of the beams, typically the beam carrying the main measurement signal, becomes tilted and deviates from the nominal interferometer topology, experiencing a longer propagation than the well aligned reference beam. The optical pathlength difference between the beams results in a phase shift that can be observed, e.g., as power fluctuations in a photodiode in a homodyne interferometer, or as a shift of the beat note's phase in a heterodyne scheme.

For example, for a lever arm tilt as shown in Figure 4, plane waves exhibit a geometric TTL coupling that can be derived from simple trigonometry to be $\frac{d}{2}\alpha^2$ to second order in α, where d is the pivot length and α the tilt angle. However, in an interferometer with real beams, the particular features of the wavefront of the interfering beams at the position of the detector come into play. Hence, TTL coupling can be observed even if the optical pathlength is unchanged by the tilt (i.e., *non-geometric* TTL coupling). For example, beam axes offsets, wavefront curvature mismatches or wavefront distortions, or, in general, effects disturbing the distribution of the phase of the overlapped optical fields in the detector surface, can be sources of non-geometric coupling.

The longitudinal pathlength signal s_{LPS} can be computed as the complex phase of the integral of the overlapped optical fields over the active area of the detector [28],

$$s_{\mathrm{LPS}} \equiv \frac{1}{k} \arg\left(\iint E_m E_r^* dA_{\mathrm{pd}} \right). \tag{1}$$

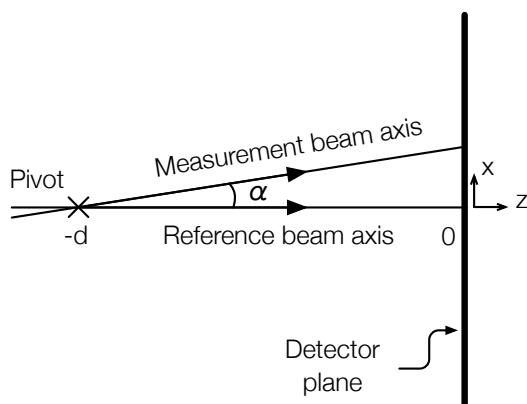where E_m is the measurement beam and E_r is the reference

FIG. 4. Lever arm tilt between two beams. Two beams (the "reference" and "measurement" beams) overlap. Their superposition is captured at a photoreceiver whose surface is the $z = 0$ plane. The measurement beam rotates about the out-of-plane y-axis and the pivot point $(0, 0, -d)^\mathsf{T}$. The tilt of the measurement beam couples into the longitudinal pathlength change sensed by the detector, which is a source of noise known as tilt-to-length coupling.
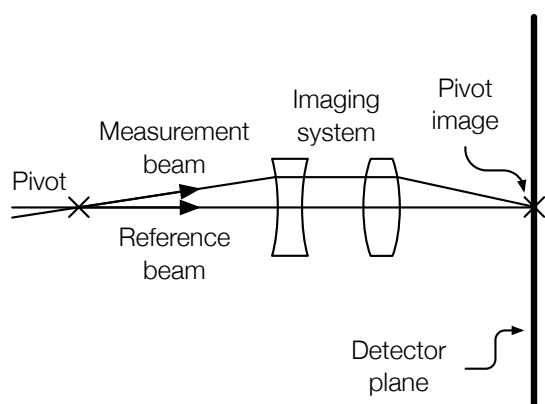

FIG. 5. TTL coupling suppression via imaging. A set of lenses is configured to image the point of rotation of the measurement beam onto the center of the detector, so that the optical pathlength is unchanged by the tilt, reducing the geometric component of the coupling of the tilt to the longitudinal pathlength sensed by the detector. A contribution will remain due to the non-geometric component, which may be counteracted by tuning the position of the detector.
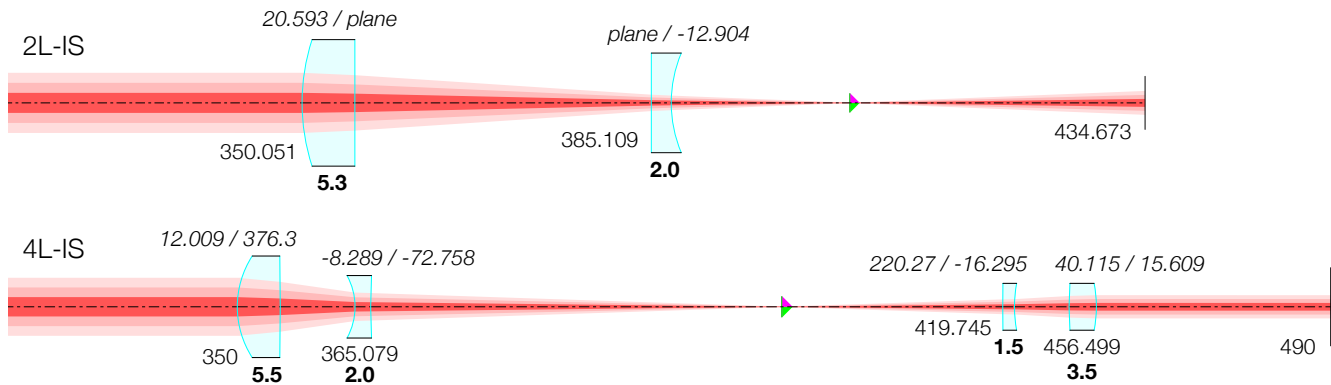
FIG. 6. Imaging systems used in the experiment. The two-lens imaging system (2L-IS) is designed by means of a computer simulation which minimizes beam walk at the photodiode for a given amount of tilt, sweeping the parameter space of the lens choice and the lens positions. The four-lens imaging system (4L-IS) is designed using a traditional ray optics approach, by tuning the system's parameters to yield a ray transfer matrix of the form given in Equation 2. The values printed on the top of the lens in italic and separated by a dash '/' represent the radii of curvature of the primary / secondary surfaces of the lens (in millimeters^{-1}). The values printed on the bottom of the lens in bold represent the thickness of the lens in the optical axis (in millimeters). The values in regular font represent the lens and detector positions (in millimeters). The position of each lens is determined by the intercept of its primary surface with the optical axis.

beam. Any dependence of s_{LPS} with beam misalignment is a source of TTL coupling. A closed expression for the LPS can be found for the case of two misaligned and mismatched Gaussian beams [29, 30] by considering a single element photoreceiver with an active area radius much larger than the Gaussian radius of the beams.

In the LA interferometer, however, the situation is somewhat more complicated. The reference beam is Gaussian, but the measurement beam is a flat-top beam that suffers diffraction due to clipping by the Rx-clip aperture found along the beam path. If this aperture is imaged onto the detector plane, the beam may be approximated by a plane wave with finite transverse extent (i.e., a flat phase-front delimited by a disk centered in the nominal optical axis). Unfortunately, even in this special case, it is not possible to express Equation 1 in terms of elementary functions, although approximate expressions may be found for the case of small misalignments.

Since the measurement beam tilts around the Rx-clip, imaging this plane onto the detector plane (Figure 5) means that the geometric component of the cross-coupling of the tilt to the longitudinal signal is minimized, leaving the contribution of the non-geometric component, as well as a residual geometric TTL coupling due to fundamental noise sources, such as thermal displacement noise. Hence, tilt-to-length coupling can be greatly reduced by placing specially tuned imaging systems in front of the photoreceivers [31].

In this paper we describe the performance of two different imaging systems for TTL coupling reduction in the LISA long-arm interferometer, a two-lens imaging system (2L-IS), and a four-lens imaging system (4L-IS). The two systems under consideration are represented in Figure 6.

Each system was designed using a different approach. The 4L-IS was designed using a classic pupil-plane imaging approach. The system is configured so that rays $(x, y, \alpha, \beta)^{\mathsf{T}}$ originating from the Rx-clip are imaged onto the detector plane with a certain magnification, $(x', y') = m(x, y)$, where (x, y)

is a point within the Rx-clip aperture, m is the magnification, and (x', y') is a point at the detector surface. This condition can be expressed using the *ray transfer matrix* formalism as

$$\boldsymbol{r'} = \begin{pmatrix} m & 0 \\ c & 1/m \end{pmatrix} \boldsymbol{r}, \qquad (2)$$

where $\boldsymbol{r} = (x, \alpha)^{\mathsf{T}}$, and we have omitted the y and β degrees of freedom due to the existing cylindrical symmetry. Note that in such system $x' = mx$ is α-invariant (i.e., rays originating at the center of the Rx-clip are projected onto the center of the photodiode). This is the fundamental condition for imaging. Moreover, the system was designed to produce a collimated output given a collimated input (i.e., $c = 0$), which makes the system more robust against beam parameter variations, and advanced techniques were used to minimize aberrations, ghosts, and the sensitivity of the system to manufacturing tolerances.

The 2L-IS was designed via numerical simulation using the interferometer modelling software IfoCAD [32, 33], and an algorithm which looks for solutions that yield minimal beam walk at the detector plane for a given amount of beam tilt and a desired magnification. The simulation consists of an optical setup such as the one described in Figure 5, introducing two lenses between the pivot point and the photodiode. The algorithm sweeps through the possible configurations of the parameter space spanned by the position and orientation of the lenses, as well as the choice of the lenses themselves. Both systems were designed to use commercially-available lenses from a popular lens manufacturer.

Note that the solutions provided by the automated approach do not necessarily fulfill the traditional characteristics of an imaging system as described by Equation 2, e.g., the resulting system's ray transfer matrix M_{ij} does not verify $M_{12} = 0$ exactly, although it is close. But the main difference between the two systems is that the two-lens system does not provide
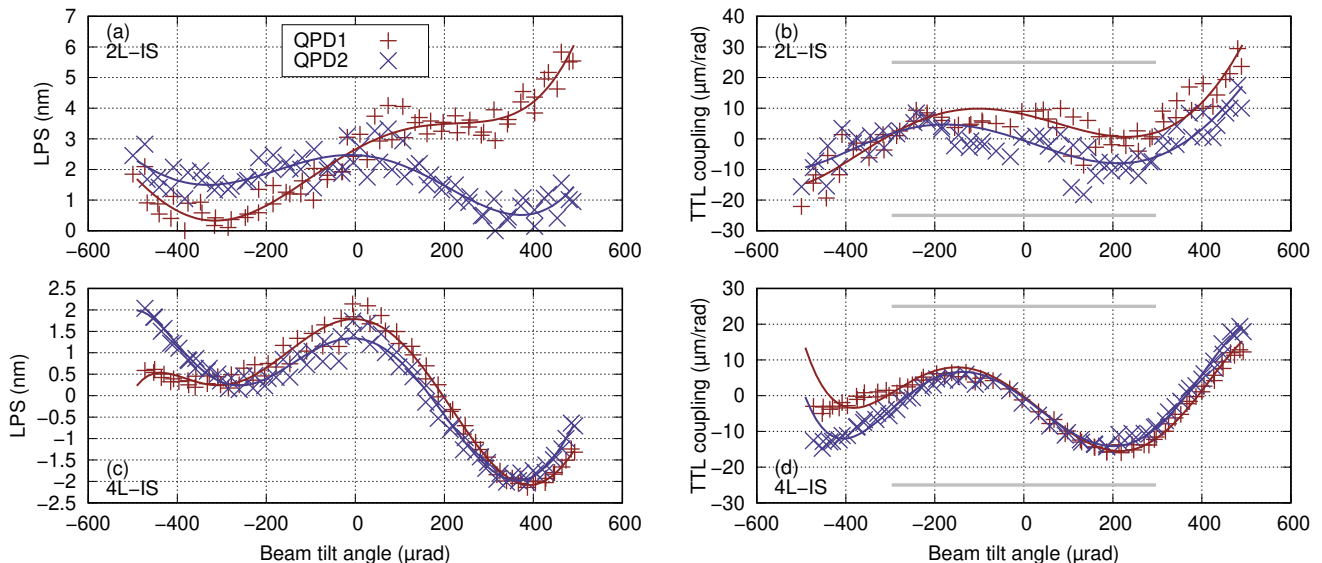
FIG. 7. Optical suppression of tilt-to-length coupling with imaging systems. The longitudinal pathlength signal from the interferometer is measured as the TS is used to induce a lever arm tilt of the measurement flat-top beam with respect to the stable reference Gaussian beam, so as to simulate angular jitter of the spacecraft in the LISA long-arm interferometer. The resulting longitudinal pathlength signal and its first derivative are plotted vs the beam tilt angle, showing that both the two-lens and the four-lens imaging systems (2L-IS and 4L-IS) perform to the required level on an optimally aligned interferometer.

a collimated output beam for a collimated input beam. The 2L-IS is known to be more sensitive to changes in the beam parameters [34, 35], although it is more robust to lateral misalignments of the components of the system itself.

The imaging systems are mounted on the OB using an optomechanical subassembly [36] that allows for precision multi-axis adjustment of the lens positions. The optical mounts of the lenses and the detectors are based on thermally stable monolithic aluminium flexures with ultra-fine precision screws allowing for $1\,\mu\text{m}$ positional precision and $<\ 1$ arcminute angular precision.

IV. RESULTS

In this section we report on the best achieved performance of the two imaging systems introduced in the previous section, as well as on their robustness to alignment deviations. For each imaging system we measure the resulting TTL coupling between the flat-top measurement beam and the Gaussian reference beam in the two quadrant photodiodes of the main measurement interferometer of the OB by introducing intentional tilts via the TS. The TS actuates on the measurement beam in a way that produces an out-of-plane tilt with respect to the Rx-clip in the optical bench (i.e., the Rx beam's propagation vector acquires a vertical component), and the relative phase between the measurement and reference beams is kept at zero at this point via the OPLLs implemented using the reference interferometer in the TS. The longitudinal pathlength signal is then obtained as a function of the beam tilt angle, and the TTL coupling is computed as the first derivative of this signal with respect to the angle.

A. Nominal performance

We first report on the nominal performance of both systems, i.e., on the measure of the achieved performance after the alignment of the system has been optimized and the TTL coupling reduced to our best effort by fine-tuning the longitudinal position of the QPDs (Figure 7). The LPS signal is obtained as the averaged phase over the four QPD segments,

$$s_{\text{LPS}}^{\text{AP}} = \frac{\psi_{\text{A}} + \psi_{\text{B}} + \psi_{\text{C}} + \psi_{\text{D}}}{4k}, \tag{3}$$

where ψ_{A} refers to the phase measured by the QPD quadrant A, and so forth. This is computed as the tilt actuators on the TS sweep the beam tilt angle. Prior to tilting the beam, the actuators find the position of the Rx beam's nominal axis. This is attained in three steps: first, a rough initial alignment is performed by commanding the actuators to move to an absolute position where contrast can be observed in the reference QPD (the amplitude-modulated Rx signal is useful for this); then, the actuators find the position which maximizes the amplitude of the heterodyne beat note between the Rx and LO beams in the reference QPD; lastly, the actuators acquire a position which minimizes the DWS signal, also in the reference QPD. This procedure is performed for both axes. After the Rx beam has been aligned successfully, the control software commands the actuators to tilt the beam from zero to the minimal and then to the maximal tilt angles.

For each step within the tilt range, the angle is measured using the calibrated DWS signals from the reference QPD in the TS, and the LPS is measured by averaging 900 samples. The TLL coupling (i.e., the first derivative of the LPS) is then
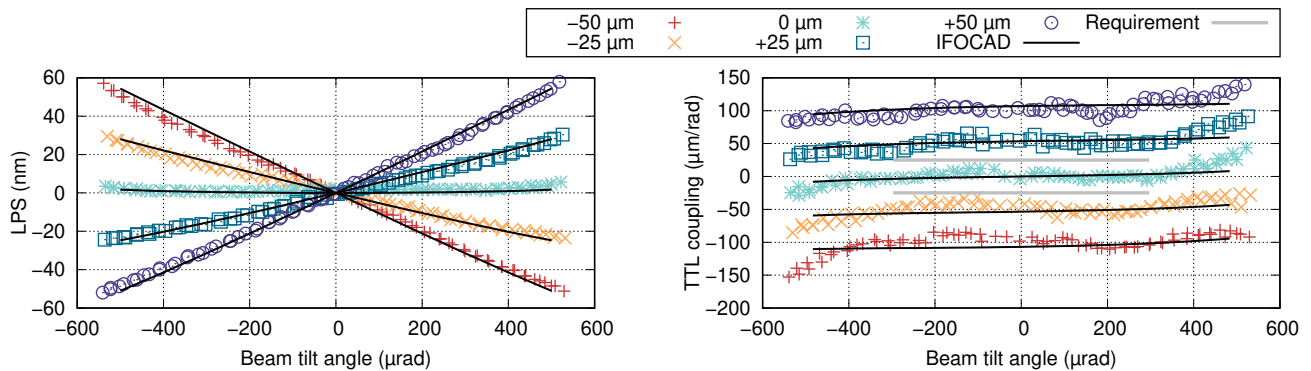
FIG. 8. Lateral shifts of the detector. Shifting the detector vertically yields a linear dependency of the longitudinal pathlength signal with the beam tilt angle and, thus, an approximately constant value in its first derivative. For example, a shift of $+25\,\mu$m of the detector translates into a TTL coupling of approximately $+50\,\mu$m/rad. The measurements are compared against numerical simulations of the experiment using IfoCAD, showing good agreement considering the precision of the alignment screw that is used to shift the QPD.

computed for each data point via a piecewise linear regression of the five neighbouring points (i.e., i, $i \pm 1$, $i \pm 2$). Both systems are able to fully meet the required specification of TTL coupling factors at or below $\pm25\,\mu$m/rad for beam tilt angles within $\pm300\,\mu$rad. The trends are shown by fitting sixth order polynomials to the data. The two-lens system exhibits slightly larger deviations from the trend, an effect that is not attributed to any differences in the system design but rather correlates with the changing environmental conditions of the testbed at the time of the measurement. The remaining TTL coupling is at or below the noise floor of the testbed, and thus a further reduction would not yield new information about the performance of the imaging systems.

B. Tolerance analysis

Having investigated the nominal performance of each imaging system, we carry out an investigation of the robustness of each system against alignment errors of the components within the systems themselves, as well as of the position of the systems relative to the testbed, in order to determine the required setup tolerances. This is a crucial step that helps us discriminate between different imaging system implementations in the future, as well as diagnose a not optimally aligned system.

The analysis is performed by introducing intentional misalignments in the testbed and measuring the resulting TTL coupling. The measurements also offer a good opportunity to verify our simulation tools by comparing the obtained results with an IfoCAD model of the experiment. The model includes the components specified in Figure 6. The reference beam is treated as a general astigmatic Gaussian beam with a 1 mm radius waist located at the pivot point (i.e., located at $(0, 0, -d)^\intercal$ as indicated in Figures 4 and 5). The reference beam parameters were measured in [34].

IfoCAD does not yet include solidly proven methods for simulating real flat-top beams. However, for a situation in which the Rx-clip is imaged onto the detector plane, the beam may be modelled as a Gaussian beam set to yield a nearly flat intensity and phase profile within the detector's active area. The detector is a quadrant photodiode with 1 mm active area diameter and $20\,\mu$m slit width.

Several degrees of freedom were investigated for both the two-lens and the four-lens systems. For example, Figure 8 shows the sensitivity of the two-lens imaging system to lateral shifts of the QPD in the vertical direction. The measurements show that a lateral misalignment of $\pm25\,\mu$m results in an additional TTL coupling of $\approx \pm50\,\mu$m/rad, and this is verified by simulation. This is in good agreement with the expected extra geometric TTL coupling resulting for a lateral shift of the detector in the direction normal to the axis of rotation of the tilting beam, which is directly proportional to the magnitude of the shift. In the presence of an imaging system, this extra coupling is scaled by $1/m$, where m is the magnification of the imaging system. The small deviation found here ($m = 4$ for the 2L-IS, so the expected geometric coupling factor is ≈ 2.5) could be due to the precision of the alignment screw that is used to adjust the lateral shift of the QPD, or an additional non-geometric effect not accounted for. The alignment screw has a pitch of $200\,\mu$m per turn and thus, e.g., a misalignment of $25\,\mu$m has an associated uncertainty of a few micrometers.

Similar investigations are carried out for all critical parameters of the system, namely the lateral alignment of each lens and the QPDs. An overview of the different tests is presented in Figure 9 for both imaging systems. Since the LPS is clearly linear in α, each point in Figure 9 is obtained as the slope of a linear regression of the LPS for a given parametric misalignment. The results are in good agreement with the IfoCAD model of the experiment, while the small deviations are likely due to the precision to which the alignment errors are estimated.

We find that the two-lens system is in general more robust to alignment errors than the four-lens system. For the four-lens system the more critical parameters are the first and second lenses, showing a maximal TTL coupling in the range of $\pm700\,\mu$m/rad for lateral shifts of $60\,\mu$m. In other words, the 4L-IS shows an effective TTL coupling sensitivity
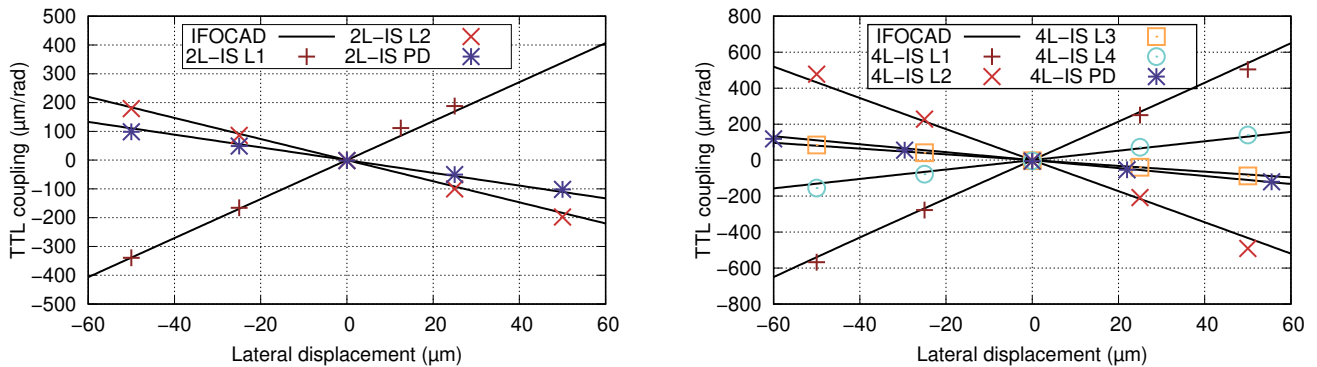
FIG. 9. Sensitivity of the interferometer to lateral shifts of the different components of the two-lens (2L-IS) and the four-lens (4L-IS) imaging systems (e.g., L1 = first lens, L2 = second lens, PD = photodetector etc). These measurements, which are derived from the slope of a linear regression of the LPS vs beam tilt angle data, agree well with the IfoCAD model of the experiment. The two-lens system offers greater robustness against alignment errors, yielding a lower TTL coupling factor for a given shift of the lenses.

of $11.5\,\text{rad}^{-1}$ to L1 and L2 alignment errors. This is in contrast with the third and four lenses of the system, both having associated sensitivities below $3.3\,\text{rad}^{-1}$. In the two-lens system, the sensitivities are $7.5\,\text{rad}^{-1}$, $4.2\,\text{rad}^{-1}$, and $2.5\,\text{rad}^{-1}$ for the first lens, second lens, and photodiode respectively.

C. Compensation by photodiode alignment

We have shown how the interferometer responds to alignment errors in the imaging systems by intentionally misaligning parts of the system. In this section we investigate how an existing misalignment can be counteracted by laterally shifting a different component. In some situations the system may not perform or be configured as expected (e.g., due to manufacturing imperfections). However, e.g., in some situations the system can be reconfigured to achieve the required performance by introducing a lateral offset to the photodiode. Thus, in an interferometer with a badly aligned imaging system yielding much larger TTL coupling than tolerable, it is often possible to compensate the system by introducing an additional lateral shift of the detector.

For example, for an alignment error of $50\,\mu\text{m}$ of the second lens in the two-lens imaging system, which yields the linear dependency of the LPS with the beam tilt angle shown in Figure 10a-b with a TTL coupling of $\sim 200\,\mu\text{m/rad}$, a realignment of the QPD to the center of the tilting measurement beam (e.g., by finding a zero crossing in the DPS signal) significantly reduces TTL coupling and returns the system to expected performance (Figure 10c-d). Moreover, a further reduction is possible by slightly shifting the QPD from the center of the measurement beam so as to minimize the residual coupling (Figure 10e-f). The same approach applies to alignment errors in the four-lens imaging system. Figure 10g-h and i-j show the effect of a vertical shift of $25\,\mu\text{m}$ of the first lens and the respective improvement by realignment of the photodiode to the center of the measurement beam, respectively.

This procedure was actually performed in order to reach the nominal performance shown in Figure 7 for both the 2L-

IS and 4L-IS systems. The imaging systems were pre-aligned during manufacturing using a different setup. In the testbed, however, it is not possible to control the beam height with precision, and thus the imaging systems were by design laterally offset from the nominal interferometer topology. Implementing the compensation of the imaging systems by photodiode alignment was therefore a critical step in order to reach performance.

V. SUMMARY AND CONCLUSION

The coupling of angular noise into the longitudinal pathlength readout is an aspect of utmost importance in space interferometers such as LISA Pathfinder, GRACE-FO, and LISA. This tilt-to-length coupling noise is considered in this paper in the context of the LISA long-arm interferometer. We have demonstrated the use of imaging systems to reduce TTL coupling in a setup representative of the LISA long-arm interferometer, a major step towards validating this noise-reduction strategy for LISA.

For this purpose an ultra-stable interferometer testbed was built, and its operation is described in Section II. The testbed was used previously to test the performance of the imaging systems in a configuration representative of the LISA test mass interferometer [34]. The testbed is a simplified version of the LISA Optical Bench, with all the components required for a TTL coupling investigation, and features a telescope simulator that provides a laser beam simulating the beam received by a LISA spacecraft. The characteristics of this measurement beam, which has a flat-top intensity and phase profile, make this interferometer unique. The telescope simulator developed for this experiment has proven to be a powerful optical ground support equipment (OGSE) candidate for the LISA Mission. A similar device may be used to aid alignment of the LISA Optical Bench and to calibrate the TTL coupling during construction.

It was shown experimentally for the two-lens and the four-lens imaging systems described in Section III that the TTL
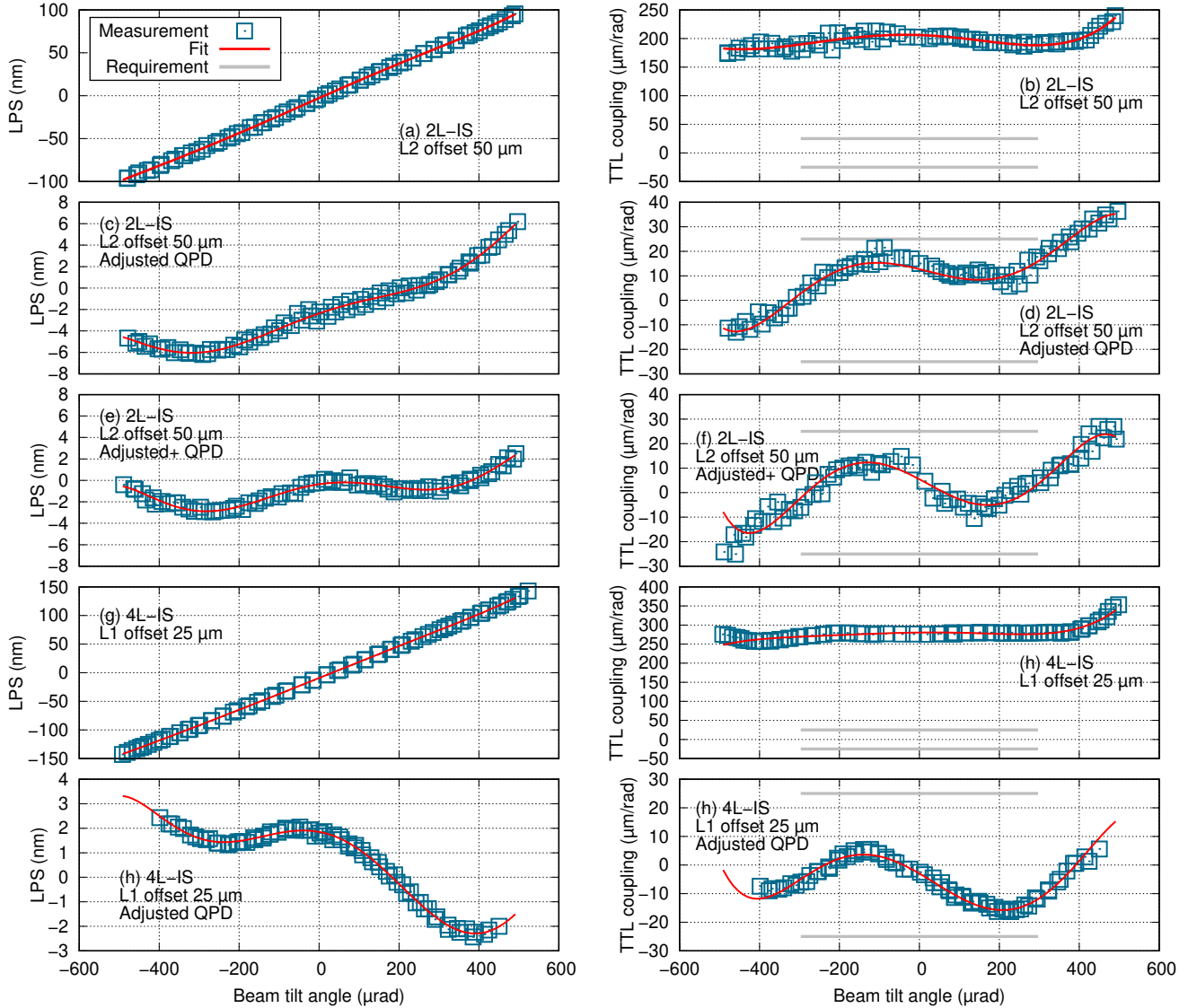
FIG. 10. Compensation of misaligned imaging systems by photodiode alignment. Plots a-b show the results of a badly aligned second lens in the two-lens imaging system, and plots c-d and e-f show the compensated system that is achieved by vertical adjustment of the QPD position (the former by centering the flat-top beam in the QPD, and the latter by slightly shifting the QPD from the center of the flat-top so as to minimize the coupling). Plots g-h and i-j show the same situation for a badly aligned first lens in the four-lens imaging system and the achieved compensation respectively.

coupling in the testbed could be reduced below the required level of $\pm 25\,\mu\text{m/rad}$ for beam tilt angles within $\pm 300\,\mu\text{rad}$ (Section IV). Furthermore, we performed a tolerance analysis of both imaging systems and investigated the additional TTL coupling due to lateral alignment errors of each system. The results obtained, in good agreement with our models, were used to demonstrate that TTL coupling can be counteracted by introducing intentional lateral shifts of other components in the system. For example, it was shown that the lateral position of the detectors could be shifted as a compensation mechanism. These findings pave the way towards the development of advanced strategies for optical TTL coupling noise

suppression in LISA.

[1] The LIGO Scientific Collaboration, Class. Quantum Grav. **32**, 074001 (2015).

[2] LIGO Scientific Collaboration and Virgo Collaboration, Physical Review Letters **116**, 061102 (2016).

[3] The eLISA Consortium, arXiv.org (2013), 1305.5720v1.

[4] P. Amaro-Seoane *et al.*, arXiv.org (2017), 1702.00786v3.

[5] M. Armano *et al.*, Physical Review Letters **116**, 231101 (2016).

[6] Armano and et al., Physical Review Letters **120**, 061101 (2018).

[7] G. Wanner, Nature Physics **15**, 1 (2019).

[8] K. Abich *et al.*, Physical Review Letters **123**, 031101 (2019).

[9] P. Amaro-Seoane *et al.*, arXiv.org (2017), 1702.00786v3.

[10] D. V. Martynov *et al.*, Physical Review D **93**, 433 (2016).

[11] G. Wanner, N. Karnesis, and L. P. collaboration, Journal of Physics: Conference Series **840**, 012043 (2017).

[12] B. S. Sheard, G. Heinzel, K. Danzmann, D. A. Shaddock, W. M. Klipstein, and W. M. Folkner, Journal of Geodesy **86**, 1083 (2012).

[13] H. Wegener, V. Müller, G. Heinzel, and M. Misffeldt, (2020, Manuscript in preparation).

[14] D. Weise, *Technical Note 6 - OB Requirements Specification and Justification*, Tech. Rep. LOB-ASD-TN-006-02 (Astrium GmbH, 2010).

[15] E. Waluschka, in *Current Developments in Optical Design and Optical Engineering VIII*, edited by R. E. Fischer and W. J. Smith (International Society for Optics and Photonics, 1999) pp. 31–39.

[16] M. V. Papalexandris and E. Waluschka, Optical Engineering **42**, 1029 (2003).

[17] C. P. Sasso, G. Mana, and S. Mottini, Classical and Quantum Gravity **35**, 185013 (2018).

[18] C. P. Sasso, G. Mana, and S. Mottini, Classical and Quantum Gravity **35**, 245002 (2018).

[19] L. d'Arcio, J. Bogenstahl, M. Dehne, C. Diekmann, E. D. Fitzsimons, R. Fleddermann, E. Granova, G. Heinzel, H. Hogenhuis, C. J. Killow, M. Perreur-Lloyd, J. Pijnenburg, D. I. Robertson, A. Shoda, A. Sohmer, A. Taylor, M. Tröbs, G. Wanner, H. Ward, and D. Weise, Proc. of SPIE **10565** (2010), 10.1117/12.2309141.

[20] A.-M. A. van Veggel and C. J. Killow, Advanced Optical Technologies **3**, 5491 (2014).

[21] E. Morrison, B. J. Meers, D. I. Robertson, and H. Ward, Appl. Opt. **33**, 5041 (1994).

[22] G. Hechenblaikner, J. Opt. Soc. Am. A **27**, 2078 (2010).

[23] M. Chwalla, K. Danzmann, G. Fernández Barranco, E. Fitzsimons, O. Gerberding, G. Heinzel, C. J. Killow, M. Lieser, M. Perreur-Lloyd, D. I. Robertson, S. Schuster, T. S. Schwarze, M. Tröbs, H. Ward, and M. Zwetz, Classical and Quantum Gravity **33**, 245015 (2016).

[24] C. J. Killow, D. I. Robertson, E. D. Fitzsimons, H. Ward, J. Hough, J. Bogenstahl, and M. Perreur-Lloyd, Applied optics **52**, 2527 (2013).

[25] G. Heinzel, V. Wand, A. García, O. Jennrich, C. Braxmaier, D. Robertson, K. Middleton, D. Hoyland, A. Rüdiger, R. Schilling, U. Johann, and K. Danzmann, Class. Quant. Grav. **21**, S581 (2004).

[26] C. J. Killow, E. D. Fitzsimons, M. Perreur-Lloyd, D. I. Robertson, H. Ward, and J. Bogenstahl, Applied optics **55**, 2724 (2016).

[27] M. Lieser, *LISA optical bench development : Experimental investigation of tilt-to-length coupling for a spaceborne gravitational wave detector*, Ph.D. thesis, Leibniz Universität Hannover (2017).

[28] G. Wanner, *Complex optical systems in space : numerical modelling of the heterodyne interferometry of LISA Pathfinder and LISA*, Ph.D. thesis, Leibniz Universität Hannover (2010).

[29] G. Wanner and G. Heinzel, Applied optics **53**, 3043 (2014).

[30] S. Schuster, G. Wanner, M. Tröbs, and G. Heinzel, Appl. Opt. **54**, 1010 (2015).

[31] S. Schuster, M. Tröbs, G. Wanner, and G. Heinzel, Optics Express **24**, 10466 (2016).

[32] IfoCAD, "http://www.lisa.aei-hannover.de/ifocad/," .

[33] G. Wanner, G. Heinzel, E. Kochkina, C. Mahrdt, B. S. Sheard, S. Schuster, and K. Danzmann, Optics communications **285**, 4831 (2012).

[34] M. Tröbs, S. Schuster, M. Lieser, M. Zwetz, M. Chwalla, K. Danzmann, G. F. Barránco, E. D. Fitzsimons, O. Gerberding, G. Heinzel, C. J. Killow, M. Perreur-Lloyd, D. I. Robertson, T. S. Schwarze, G. Wanner, and H. Ward, Classical and Quantum Gravity **35**, 105001 (2018).

[35] S. Schuster, *Tilt-to-length coupling and diffraction aspects in satellite interferometry*, Ph.D. thesis, Leibniz Universität Hannover (2017).

[36] M. Perreur-Lloyd, K. Danzmann, E. D. Fitzsimons, G. Heinzel, J.-S. Hennig, C. J. Killow, M. Lieser, D. I. Robertson, S. Schuster, A. Taylor, M. Tröbs, H. Ward, and D. Weise, Journal of Physics: Conference Series **610**, 012032 (2015).